

https://dspace.org/

Switching Events of Wakes Shed From Two Short Flapping SidebySide Cylinders

Yong Pu Wang; Michael Atkins; Tian Jian Lu; Tong Kim

ASME
https://hdl.handle.net/10539/45584
WOS

Downloaded from a DSpace repository. https://dspace.org/

Check for updates

ASME Journal of Fluids Engineering
Online journal at:
https://asmedigitalcollection.asme.org/fluidsengineering

Yong Pu Wang
College of Aerospace Engineering,
Nanjing University of Aeronautics and Astronautics,
Nanjing, Jiangsu Province 210016, China
e-mail: ypwang@nuaa.edu.cn

Michael D. Atkins[1]
School of Mechanical, Industrial and Aeronautical Engineering,
University of the Witwatersrand,
Johannesburg 2000, South Africa
e-mail: Michael.Atkins@wits.ac.za

Tian Jian Lu
College of Aerospace Engineering,
Nanjing University of Aeronautics and Astronautics,
Nanjing, Jiangsu Province 210016, China
e-mail: tjlu@nuaa.edu.cn

Tongbeum Kim[1]
College of Aerospace Engineering,
Nanjing University of Aeronautics and Astronautics,
Nanjing, Jiangsu Province 210016, China
e-mail: tongbeum.kim@nuaa.edu.cn

Switching Events of Wakes Shed From Two Short Flapping Side-by-Side Cylinders

The wakes shed alternatively from two long stationary side-by-side cylinders have long been an issue in many engineering applications, such as wind energy harvesting schemes that utilize vortex-induced vibrations (VIVs). In this study, switching events of the wakes shed from two "short," "flapping" side-by-side cylinders are investigated. To this end, the flow visualization and spectral analysis of the time-resolved data from hot-wire anemometers and the piezoelectric mount of flapping cylinders are carried out. Measurements are conducted with differing center-to-center spacing normalized by a single cylinder diameter (T/D)—gap ratio, and length-to-diameter ratio (L/D) in a Reynolds number range of $800 \leq Re_D \leq 16{,}000$*. The results demonstrate the transition of wake shedding patterns, sequentially from a single bluff body wake, first bistable wakes, tristable wakes, second bistable wakes, and eventually to coupled wakes as the gap ratio is increased. Furthermore, the role of shortness and flapping of the two cylinders in determining the wake kinematics is elucidated, and the transitional sequences and switching of dominant shedding frequencies are detailed.*
[DOI: 10.1115/1.4067191]

1 Introduction

Flow around two circular cylinders in a side-by-side arrangement is of practical significance in many branches of engineering, e.g., the design of nuclear reactor cores, offshore drilling platforms, heat exchanger tube bundles, and power transmission lines [1–3]. It is also relevant to a renewable energy harvesting scheme where flow past structural bodies induces motion, thus extracting associated kinetic energy [4]. The fluid–structure interaction is correlated with the wake shedding behavior, and the associated unsteady fluid forces that drive the structural vibration. The resultant structural vibration, in turn, affects the vortex shedding behavior, giving rise to two-way-coupled interactions. Thus, this study aims to understand (i) the wake shedding of two side-by-side cylinders, (ii) the corresponding cylinders' vibration behavior, and (iii) the mutual interaction between wake shedding and structural vibration.

Flow characteristics around two side-by-side cylinders are dependent on geometric and fluidic parameters including (i) the center-to-center distance, T/D with D being the cylinder diameter, often termed "gap ratio" or gap spacing [5,6], (ii) end conditions [7,8], (iii) surface roughness [9], (iv) pressure gradients [7,10], (v) freestream turbulence [11], and (vi) Reynolds number (Re_D) [12]. Wakes shed from two "long" side-by-side cylinders are two-dimensional. Based on the analysis of vortex shedding frequencies, three wake regimes have been broadly classified as their gap ratio is varied [1,2,13–18]: (i) single bluff body wake regime (in Fig. 1(*a*)), (ii) biased wake regime (in Fig. 1(*b*)), and (iii) coupled wake regime (in Fig. 1(*c*)).

Specifically, the single bluff body wake regime is defined (Fig. 1(*a*)) when the gap ratio is small, e.g., $T/D < 1.1$–1.2, including cylinders in contact (i.e., $T/D = 1.0$) [2,15–17,19]. An asymmetric single vortex street is formed with alternating vortices shed from the outer surfaces of two closely positioned cylinders as if being shed from a single bluff body of $D_e = 2D$ [2,20].

In a gap ratio range of 1.1–$1.2 \leq T/D \leq 2.0$–2.2, the bistable wake regime is classified (Fig. 1(*b*)) by asymmetric wake patterns where the gap flow is biased toward one of the two cylinders with switching [13,17,21]. A narrow wake that has a higher shedding frequency is formed when the gap flow is deflected toward a given cylinder while the corresponding cylinder has a wide wake that is shed at a lower frequency. Another dominant frequency was also noted, lying between narrow and wide wakes [13,19,20], identified as an intermediate wake whose wake shedding frequency is almost equal to that of a single cylinder [19]. Before and after the switching, both narrow and wide wakes remain, with a duration that is a few orders of magnitude longer than the vortex shedding period [22]. Kim and Durbin [23] confirmed that the switching is a Poisson stochastic process, indicating its randomness.

The coupled wake regime begins with a higher gap ratio, e.g., 2.0–$2.2 < T/D < 4.0$–4.5 as shown in Fig. 1(*c*) [2,14]. Here, the proximity interference of two side-by-side circular cylinders leads to antiphase and in-phase wake shedding modes as shown in Fig. 2. The typical, coupled wake shedding pattern is the symmetrical,

[1]Corresponding authors.

Contributed by the Fluids Engineering Division of ASME for publication in the Journal of Fluids Engineering. Manuscript received July 29, 2024; final manuscript received October 29, 2024; published online December 9, 2024. Assoc. Editor: Timothy Lee.

 Copyright © 2025 by ASME

Downloaded from http://asmedigitalcollection.asme.org/fluidsengineering/article-pdf/147/5/051301/7413435/fe_147_05_051301.pdf by University of Witwatersrand - Wartewieler Library user on 01 July 2025

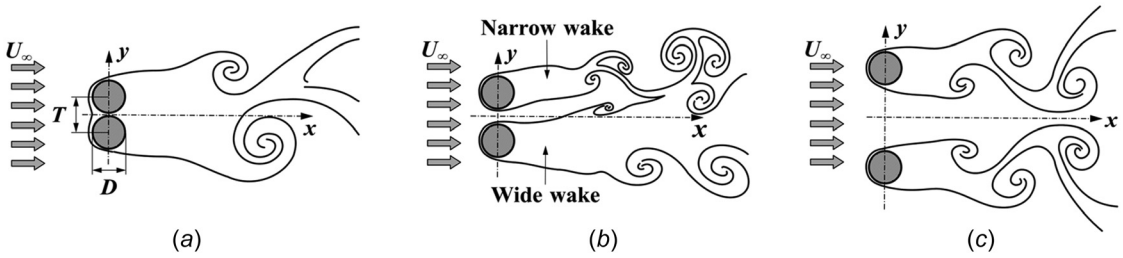


Fig. 1 Schematic representation of distinct wake regimes varying with gap ratio: (*a*) single bluff body wake regime, $T/D < 1.1–1.2$ [2,16–18]; (*b*) bistable wake regime, $1.1–1.2 \le T/D \le 2.0–2.2$ [1,18,19]; and (*c*) coupled wake regime, $2.0–2.2 < T/D < 4.0–4.5$, at $30–48 \le Re_D < 500{,}000–1{,}000{,}000$ [2,15]

"antiphase" mode in Fig. 2(*a*) where the wake shedding pattern behind each cylinder is mirrored with respect to the centerline axis of the two cylinders, such that vortices are shed simultaneously on both sides of the gap between the cylinders [16,17,24,25]. Wakes from both cylinders are shed at the same frequency, which eventually approaches the values of a cylinder in isolation. The synchronized vortex shedding wake pattern indicates significant coupling between the two cylinders. Another wake shedding pattern appears where the outer vortices of two cylinders are shed alternately by a phase difference of half a shedding period—"in-phase" mode (Fig. 2(*b*)).

Alternating vortices that are shed in the wake create periodic pressure variations on the cylinder surfaces and fluidic forces (i.e., lift and drag). In turn, vibration is generated, called "vortex-induced vibration" (VIV) if the cylinder has degrees-of-freedom in the plane which is perpendicular to the axis of the cylinder span. The dynamic characteristics of the vibrating cylinder are dependent on the reduced velocity, mass-to-fluid mass ratio, stiffness, damping, to influence the fluid–structure interaction phenomena [26,27].

A slender elastic cylinder has multiple natural frequencies along the span so different directions are available for vibration. In the transverse direction, the fluidic excitation force is caused by periodic lift (or side) force resulting from the vortex shedding, with the same frequency as the vortex shedding f_s. In the direction parallel to the flow or also called "in-line VIV," the dominant frequency is twice that of f_s, relevant to the drag force [28]. Most research has focused on one-dimensional crossflow VIV of a circular cylinder for which the transverse response is typically the largest [29–31]. Furthermore, the in-line VIV is considered negligible in air due to the significantly lower vibration amplitude [32].

The VIV of an "elastically mounted cylinder," represented by a spring–mass system subjected to crossflow, serves as the first step toward understanding more complicated VIV related features [30,33–35]. Important variables identified for stiff cylinders to be the critical damping and the ratio between structural mass and displaced fluid mass—the mass ratio. A product of the mass ratio and the damping constant determines the magnitude of transverse displacements; a large value of the product in air induces a small vibrational amplitude, in contrast to two or three orders of larger vibrational amplitudes in water [29,36]. Especially, when the VIV frequency matches the natural frequency of the elastic cylinder, the vibrational amplitude increases suddenly due to the resonance [33].

While the foregoing investigations have greatly improved our understanding of fluid dynamics around a single stationary rigid cylinder, very few studies exist on the VIV of two cylinders in a side-by-side arrangement. These two cylinders with coupled vibration behaviors can exhibit synchronization in the direction of vibration, where the two cylinders vibrate at the same frequency. Antiphase and in-phase vibration modes are illustrated in Fig. 3, showing that the typical vibration behavior of two cylinders is reflected in the coupled vibration phase. Antiphase vibration mode is defined when the two cylinders undergo a transverse motion synchronously in opposite directions (Fig. 3(*a*)). Figure 3(*b*) shows the in-phase vibration mode, with the synchronized cylinder transverse motion that is in the same direction. The side-by-side arranged cylinders have produced three different wake shedding regimes in the interference region, i.e., single bluff body regime, bistable regime, and coupled wake shedding regime, which would lead to different vibration behaviors if two cylinders are available to vibrate.

Single bluff body regime excites an in-phase oscillation of both cylinders [14,37,38]. In the bistable regime, two distinct vibration modes are observed, i.e., antiphase cylinder vibration induced by narrow wakes and in-phase vibration by wide wakes all via resonance [37,38]. Kim and Alam [10] conducted a free-vibration experiment in air to examine the VIV responses of two short side-by-side "elastically mounted" circular cylinders at $T/D = 1.1–4.2$. They further found that the bistable regime extended ($1.2 \le T/D < 3.1$) due to cylinder vibration. With the gap ratio between $1.2 \le T/D \le 1.9$, the gap flow acting as a base-bleeder suppressed the vortex formation, leading to unnoticeable vibration for either cylinder. However, when the gap ratio increased to $1.9 < T/D < 3.1$, bistable gap flow switching and increased vibration of the two separated cylinders were observed where the amplification of the vibration was caused by resonance. A further increase of the gap ratio, $3.1 \le T/D \le 4.2$, caused the two cylinders to feature the same vibration characteristics as an isolated cylinder.

A group of short rigid cylindrical structures arranged in a side-by-side manner with one end fixed and the other end being free to vibrate about a single "flapping axis" is a practical setup that is used for wind or hydro energy harvesting. In this study, the setup is termed "flappable," which consists of a rigid circular cylindrical bluff body with one end connected to a substrate by a plate piece while the other end is free to vibrate transversely. During flapping, only the plate piece undergoes elastic bending. This setup is different from the translational motion of elastically mounted rigid cylinders. For the vortex shedding induced vibration of these

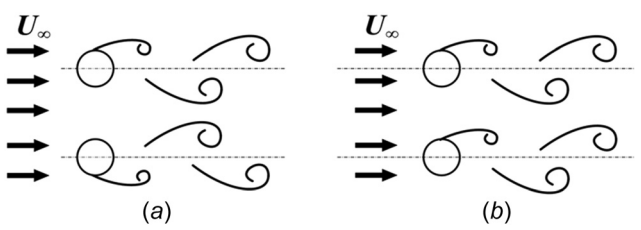


Fig. 2 Synchronized vortices shed from two long side-by-side cylinders: (*a*) antiphase mode and (*b*) in-phase mode

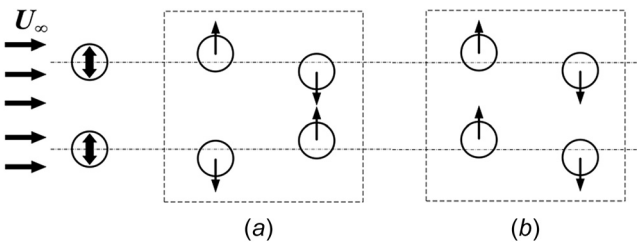


Fig. 3 Vibration modes of two long side-by-side cylinders: (*a*) antiphase mode and (*b*) in-phase mode

Downloaded from http://asmedigitalcollection.asme.org/fluidsengineering/article-pdf/147/5/051301/7413435/fe_147_05_051301.pdf by University of Witwatersrand - Wartewieler Library user on 01 July 2025

flappable cylinders, we adopt a term, "vortex-induced flapping." Despite the importance of this setup for harvesting wind energy by two or more side-by-side circular piezo-sensors, no published work thus far has attempted to characterize and understand the wake shedding and vibrational flapping motion and their interaction. Thus, we aim to experimentally investigate the kinematics of vortices in wakes shed alternatively from two short circular side-by-side flappable cylinders immersed in airstream. Focus is placed on the biased, bistable, and tristable behaviors that are influenced by a center-to-center distance (gap ratio) between the two flappable cylinders. A series of measurements in a blowdown wind-tunnel was carried out by using hot-wire anemometers in a range of $800 \leq \mathrm{Re}_D \leq 16{,}000$ and by visualizing wake patterns at $\mathrm{Re}_D = 1800$.

2 Experimental Details

2.1 Test Facility. The wake shedding and cylinder flapping characteristics of two short flappable circular cylinders in a side-by-side arrangement were experimentally quantified. To this end, a purposely designed test rig that consisted of a blowdown wind-tunnel and rectangular test section accommodating stationary and flappable cylinders was constructed as shown in Fig. 4(*a*).

The wind-tunnel has a rectangular test section of $w = 480$ mm and $h = 100$ mm. Air at ambient conditions was driven by a centrifugal blower of 7.5 kW and passed through a set of grid meshes and honeycombs. A frequency inverter controlled the blower speed so that the Reynolds number based on a single cylinder with diameter $D = 20$ mm could be varied from 800 to 16,000.

The tested objects, including the stationary and flappable cylinders, are mounted on the test section's upper wall. Tested cylinders had a diameter of $D = 20$ mm and length of $L = 99$ mm to provide 1.0 mm clearance gap for the cylinder's free end from the test section lower wall. Cylinders were made of a photosensitive resin by 3D printing. Other stationary cylinders with the L/D ratio of 10.0 and 38.5 were also fabricated by varying the diameter while the length was fixed to be $L = 99$ mm.

The mounting of the flappable cylinder consisted of a bendable plate to allow flapping motion of the cylindrical body with respect to the flapping axis indicated in the inset of Fig. 4(*a*). The bendable mounting comprised of a lead zirconate titanate (PZT) ceramic bimorph plate (size of 20 mm × 8 mm × 0.8 mm) and was fixed to the base through the PZT plate with the length of $a = 8$ mm (i.e., the distance between the cylinder bluff body and the base). For the side-by-side arrangement, the center-to-center spacing (gap ratio) of two parallel cylinders was systematically varied as illustrated in Fig. 4(*a*). Flappable cylinders are free to flap without contacting the test section wall, generating piezoelectric voltage (V_p) signals that were connected to a data acquisition system (DL350, YOKOGAWA, Tokyo, Japan) at a sampling rate of 2 kHz. The acquired voltage signals allow for the spectral and phase analysis of the flapping cylinder's vibrational characteristics. In addition, a laser displacement sensor (KEYENCE, IX-055, lmwood Park, NJ) was used to measure the flapping displacement of an isolated cylinder midspan for a sampling time of 100 s. Based on the time-resolved data of midspan displacement, the flapping angle (ε) was obtained by trigonometric calculations as shown in Fig. 5(*a*), and the root-mean-square (RMS) value of flapping angle ($\varepsilon_{\mathrm{RMS}}$) was determined. Figure 5(*b*) shows a linear relationship between the RMS flapping angle ($\varepsilon_{\mathrm{RMS}}$) and the RMS voltage ($V_{p,\mathrm{RMS}}$) signal generated by the PZT plate.

2.2 Time-Averaged and Time-Resolved Velocity Measurements. The distribution of velocity of the mainstream along the height and width of the test channel 10D upstream from the axis of the cylinders were measured by a Pitot tube (L-type, 3.0 mm diameter) (see the inset of Fig. 4(*a*)). Two linear traverse systems were used to incrementally traverse the Pitot tube that was connected to a digital micromanometer (TSI 9565-P-NB). The flow velocity was recorded at a sampling rate of 1 Hz for 60 s, resulting in a time-averaged velocity. The velocity data were normalized by the channel center value, i.e., U_c and plotted in Fig. 4(*b*), which shows velocity profiles typical in a rectangular channel.

To quantify the level of turbulence in the mainstream by turbulence intensity (T_i), time-resolved velocity was measured at the same plane as the time-averaged velocity by the Pitot tube, using a single velocity component hot-wire probe (55P11, Dantec Dynamics™, Skovlunde, Denmark) and data acquisition system (CTA-Streamware Pro MultiCal, Dantec Dynamics™, Skovlunde, Denmark). During measurements, the time-resolved voltage signals associated with the fluctuating flow velocity were acquired at a sampling rate of 20 kHz for 60 s, resulting in a total of 1,200,000 samples.

The root-mean-square of the mainstream velocity (U_{RMS}) was defined as

$$U_{\mathrm{RMS}} = \sqrt{\frac{1}{N}\sum_{i}^{N}(U')^2} \tag{1}$$

where N represents the number of signal samples, $U' = U - \bar{U}$ denotes the instantaneous mainstream velocity fluctuation, U is the measured instantaneous velocity at a given point of interest, and $\bar{U}$ is the time-averaged velocity. Turbulence intensity was obtained by normalizing the root-mean-square velocity by the time mean velocity as

$$T_i = U_{\mathrm{RMS}}/\bar{U} \tag{2}$$

Figure 4(*c*) shows the variation of T_i with the mainstream velocity in the test channel. T_i was approximately 1.5% at $U_\infty = 1.0$ m/s and yet gradually increased with increasing U_∞ until $U_\infty = 4.0$ m/s with a slight fluctuation. On the other hand, at a higher range, e.g., $U_\infty \geq 4.0$ m/s, the turbulence intensity became largely constant having the value of $T_i = 2.75\%$, quantified by the two hot-wire anemometer probes (HWA #1 and #2).

Prior to measurements, calibration was carried out for a range of velocities, ranging from 2.5 to 18 m/s in 0.5 m/s increment using a jet stream-type calibrator, StreamLine Pro Automatic Directional Calibrator, Dantec Dynamics™, Skovlunde, Denmark, such that the voltage and velocity could be correlated using King's law [39], as

$$E^2 = A + B \cdot U^n \tag{3}$$

where E is the voltage signal of each probe, A and B are dimensionless coefficients, and U is a given velocity. King [39] suggested $n = 0.5$, but a better curve fit was obtained with $n = 0.45$ by Collis and Williams [40]. For the current calibration, $n = 0.45$ was adopted. The result showed that E^2 and $U^{0.45}$ could be linearly fitted (0.9% error), with $A = 1.54$ and $B = 0.88$.

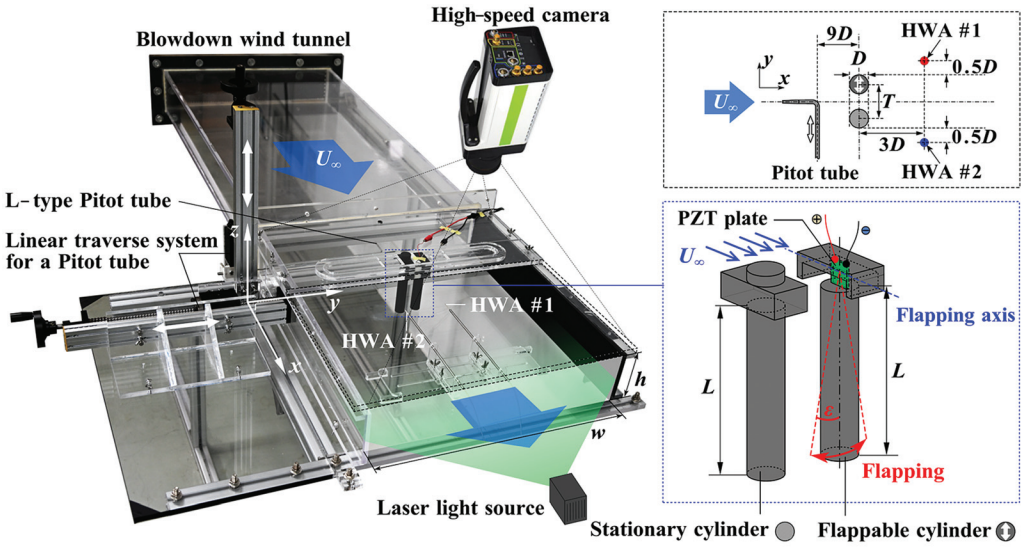
To identify the frequency characteristics of wakes shed from stationary and flappable cylinders, time-resolved measurements were also carried out. For this purpose, a total of two hot-wire probes were used with each positioned behind the test specimens as indicated by the inset of Fig. 4(*a*). The hot-wire signals were processed using a fast Fourier transform to convert discrete signals from the time domain to frequency domain. As a result, dominant frequencies could be determined in the form of Strouhal number defined as

$$\mathrm{St} = \frac{f_s D}{U_\infty} \tag{4}$$

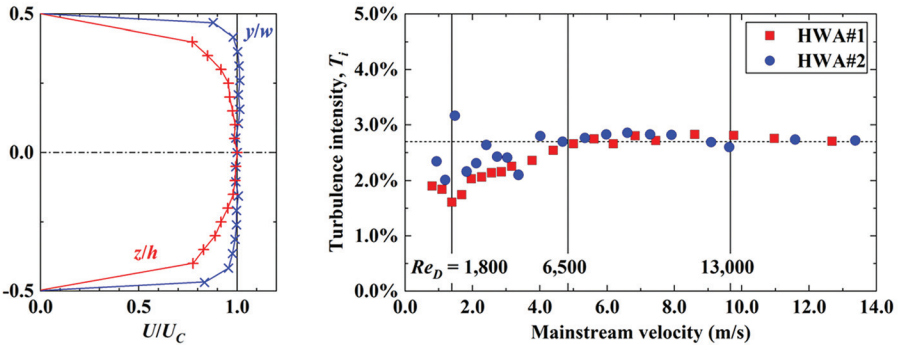
where f_s is the dominant wake shedding frequency identified from the power spectra by fast Fourier transform, D is the single cylinder diameter, and U_∞ is the time mean mainstream velocity.

2.3 Flow Visualization. A smoke-wire technique was used to visualize wake shedding patterns in the wind-tunnel where the air stream is visualized by evaporating a smoke-generating substance, i.e., paraffin from a fine heat resistance wire by means of electric

Downloaded from http://asmedigitalcollection.asme.org/fluidsengineering/article-pdf/147/5/051301/7413435/fe_147_05_051301.pdf by University of Witwatersrand - Wartewieler Library user on 01 July 2025



(*a*)

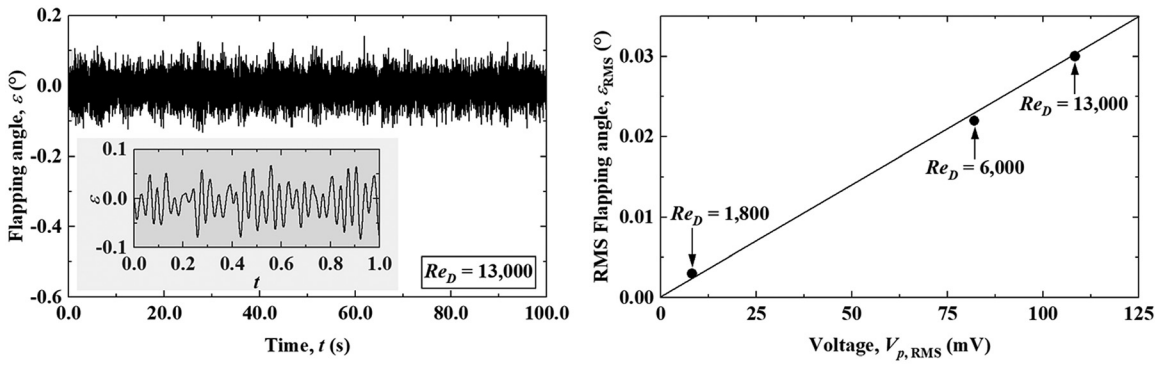


(*b*) (*c*)

Fig. 4 Test setup showing a blowdown wind-tunnel and rectangular test section with two hot-wire anemometer (HWA) probes and a Pitot tube instrumented: (*a*) schematic, (*b*) velocity profiles in both *x*- and *y*-axis planes, and (*c*) mainstream turbulence

heating, to create a "smoke rake." The nickel–chromium wire of 0.2 mm diameter was selected as the heating wire with a 0.5 mm diameter cotton thread embedded with paraffin-waxed wrapped around. During heating, the paraffin-wax melts in the cotton thread to create discrete, small drops that also vaporize to produce smoke streams emanating from the heating wire as a "rake" of streamlines. A variable transformer was used to regulate the voltage applied to the nickel–chromium wire thus generating smoke. The smoke wire was installed 5 diameters upstream of the tested cylinders horizontally in the cylinders' midspan plane and was supported by small springs at both ends to keep its tension. To avoid flow interference, all electrical connections were located outside of the test section.

The airflow that carried the paraffin smoke stream was illuminated with a light source (Mitsubishi MTO M334520-W-G laser, Tokyo, Japan) positioned in the far wake downstream of the



(*a*) (*b*)

Fig. 5 Variation of an isolated cylinder flapping displacement: (*a*) flapping angle variation with time and (*b*) variation of RMS flapping angle versus PZT plate voltage

Downloaded from http://asmedigitalcollection.asme.org/fluidsengineering/article-pdf/147/5/051301/7413435/fe_147_05_051301.pdf by University of Witwatersrand - Wartewieler Library user on 01 July 2025

test section (Fig. 4(*a*)). Visualized flow images were captured with a high-speed camera (i-speed 720, IX Cameras, Rochford, UK) at the rate of 100 frames per second, that is roughly ten times faster than the observed wake shedding frequency.

2.4 Cylinder to Fluid Mass Ratio. As a key parameter of vortex-induced vibration, a cylinder-to-fluid mass ratio is defined [14] as

$$m^* = \frac{m}{\rho(D/2)^2} \tag{5}$$

where m is the per unit length mass of the cylinder part immersed in the fluid, D is the cylinder diameter, and ρ is the air density. The calculated m^* of the tested flappable cylinder assemblies (the piezoelectric (PZT) plate and rigid cylinder) is 1240 and 1430 with the natural frequency of 30 Hz and 31 Hz, damping expressed as a logarithmic decrement of 0.017 and 0.016, respectively, for flappable cylinder #1 and flappable cylinder #2.

2.5 Measurement Uncertainties. Measurement uncertainties were estimated using a method detailed in the literature [41], as follows. If $y = f(x_1, x_2, \ldots, x_n)$, then the uncertainty propagated by x_i in the variable y is given by

$$\Delta y = \sqrt{\left(\frac{\partial y}{\partial x_1}\Delta x_1\right)^2 + \left(\frac{\partial y}{\partial x_2}\Delta x_2\right)^2 + \cdots + \left(\frac{\partial y}{\partial x_n}\Delta x_n\right)^2} \tag{6}$$

where Δx_i is the absolute uncertainty in x_i. Equation (6) was used in this study to estimate overall experimental uncertainties associated with vortex shedding frequency and velocity measurements.

The measurement uncertainty of the Reynolds number, axial flow velocity, and RMS piezoelectric voltage signal were estimated for a confidence level of 95% to be within 1.6%, 1.6%, and 2.3%, respectively. Here, the uncertainty of the cylinder dimensions and transverse center-to-center cylinder spacing was within ±0.03 mm. The pitot tube traverse positions along the z- and y-axis were measured using a digital caliper that was mounted onto the linear traverse system, having a resolution of 0.01 mm. The resolution of vortex shedding frequency measured by a hot-wire anemometer is within ±2.8 Hz, and thus the corresponding uncertainty in the Strouhal number was estimated to be 4.3%.

3 Discussion of Results

We aim to understand the wake shedding behavior and vibrational characteristics of two short cylinders in a side-by-side arrangement that are subjected to vortex-induced flapping motion due to external airstreams. To this end, wake shedding characteristics were determined by a series of spectral analyses based on the time-resolved data from hot-wire anemometers placed in the wake for varied gap ratios in conjunction with visualized images. To systematically decouple effects of (i) shortness, (ii) transverse proximity (center-to-center spacing, often termed gap ratio, T/D), and (iii) flapping, the test configurations are arranged as follows: (a) an *isolated* stationary cylinder with varying length-to-diameter (aspect) ratio, (b) two *long* stationary cylinders in a side-by-side arrangement, (c) two *short* stationary cylinders in a side-by-side arrangement, and (d) two short *flapping* cylinders in a side-by-side arrangement. Furthermore, the flapping characteristics of the short cylinders were measured via the generated piezoelectric plate voltage signals (V_p). A new classification of wake shedding from two short flapping cylinders in a side-by-side arrangement will be made, and new insight into the intrinsic switching events will be detailed for differing gap ratios in the Reynolds number range of $800 \leq \mathrm{Re}_D \leq 16{,}000$.

3.1 Wake Shedding From a Cylinder in Isolation. In a weak fluid stream, e.g., Reynolds numbers below 50, there is no wake shed from a long cylinder. With increased airstream velocity, alternating wakes begin to shed from both sides of the cylinder. As characterized nondimensionally by the Strouhal number (defined in Eq. (4)), the initially low shedding frequency increases as the airstream velocity is increased in Fig. 6(*a*). Roughly after $\mathrm{Re}_D = 300$, the Strouhal number becomes independent of the Reynolds number, being $\mathrm{St} \sim 0.21$ [42]. Our experimental data for a length-to-diameter ratio (termed an "aspect ratio") of $L/D = 38.5$ in $600 \leq \mathrm{Re}_D \leq 8000$ agree well with the widely accepted Strouhal number dependence on the Reynolds number [42]. The relatively short cylinders, e.g., $L/D = 5.0$ and 10.0, show that the wake shedding frequency of these two shortened isolated cylinders has reduced, being $\mathrm{St} \sim 0.14$ and 0.15, respectively. The effect of the cylinder flapping motion on the wake's shedding frequency is also shown in Fig. 6(*a*). Here, an isolated short ($L/D = 5.0$) cylinder that can flap is shown to further reduce the shedding frequency, $\mathrm{St} \sim 0.13$. The flapping cylinder displacement is limited, e.g., the RMS value of flapping angles $\varepsilon_{\mathrm{RMS}} \approx 0.003$ deg at $\mathrm{Re}_D = 1800$ and is 0.03 deg at $\mathrm{Re}_D = 13{,}000$ (see Fig. 5(*b*)), which is attributed to the product of mass ratio and damping $m^*\xi$ being high [35]. For all the cases tested, the Strouhal number is largely independent of the Reynolds numbers, from $\mathrm{Re}_D = 2000$ to 16,000.

To quantify the effects of L/D on shedding frequencies, the data from the present study and previous studies [8,42–44] at selected Reynolds numbers are collated in Fig. 6(*b*). All data points consistently show that as the aspect ratio is increased, the Strouhal number is increased, approaching an asymptotic value, $\mathrm{St} \sim 0.21$, approximately after $L/D = 20.0$ [2,12,19]. This confirms the reduced vortex shedding frequencies caused from shorter cylinders in isolation [45]. With the shortened aspect ratio ($L/D = 5.0$), the single cylinder flapping motion further reduces the wake shedding frequency (see Fig. 6(*a*)).

3.2 Wake Shedding From Two Long Stationary Side-by-Side Cylinders. Next, we consider two long cylinders that are in a side-by-side arrangement. Figure 7 shows the variation of the Strouhal number with the center-to-center distance between the cylinders—gap ratio (T/D). For $T/D < 1.2$, the two cylinders behave like a single bluff body having an equivalent diameter of $D_e = 2D$, giving rise to $\mathrm{St} = f_s D_e/U_\infty \sim 0.21$, consistent with the widely accepted Strouhal number. In $1.2 \leq T/D < 2.2$, referred to as the biased (or bistable) wake regime, the majority of previous studies [22,23,46] observed two dominant Strouhal numbers, each corresponding to wide and narrow wakes. Here, vortices shed from the wide wakes have a lower shedding frequency, while a higher shedding frequency exists in the narrow wakes.

On the other hand, a few studies including Bearman and Wadcock [13] and Spivack [20] found a third dominant frequency in the bistable wake regime that correlates to an intermediate value for the Strouhal number between the narrow and wide wakes. The corresponding intermediate Strouhal number is equivalent to that for a cylinder in isolation, $\mathrm{St} = f_s D/U_\infty \sim 0.21$ based on the single cylinder diameter. Our experimental data support the existence of the third, intermediate wake shedding frequency in this T/D range as plotted in Fig. 7. We denote this as an intermediate Strouhal number, $\mathrm{St}_{\mathrm{int}}$. For example, at $T/D = 1.7$, the higher St is about $1.5\,\mathrm{St}_{\mathrm{int}}$, while the lower St is roughly $0.5\,\mathrm{St}_{\mathrm{int}}$. As the gap ratio increases, approaching $T/D \sim 2.2$, the present study reveals three co-existing Strouhal numbers. However, increasing the gap ratio further toward $T/D = 2.2$ causes these higher and lower Strouhal numbers to merge to the intermediate Strouhal number, which remains largely unchanged. After $T/D = 2.2$, the single Strouhal number persists, having $\mathrm{St} \sim 0.21$, referred to as the coupled wake regime.

Thus far, the present study has confirmed that three distinct gap ratio regimes exist as shown in Fig. 7. When the two side-by-side cylinders are near to each other, the wake pattern mimics a single bluff body indicated as *regime I*. With the two side-by-side cylinders sufficiently far from each other, the coupled symmetric wake regime is established (i.e., *regime III*). Between these two regimes, *tristable*

Downloaded from http://asmedigitalcollection.asme.org/fluidsengineering/article-pdf/147/5/051301/7413435/fe_147_05_051301.pdf by University of Witwatersrand - Wartewelier Library user on 01 July 2025

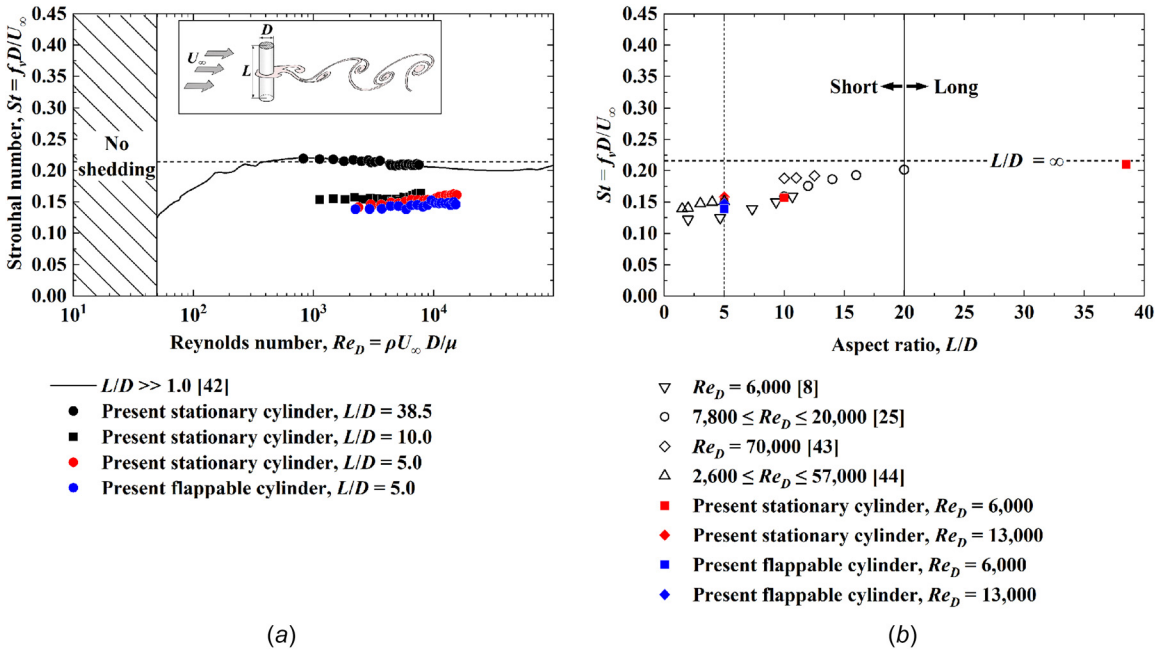


Fig. 6 Wakes shed from a cylinder in isolation: (*a*) Strouhal number varying with Reynolds number and (*b*) effect of aspect ratio on Strouhal number

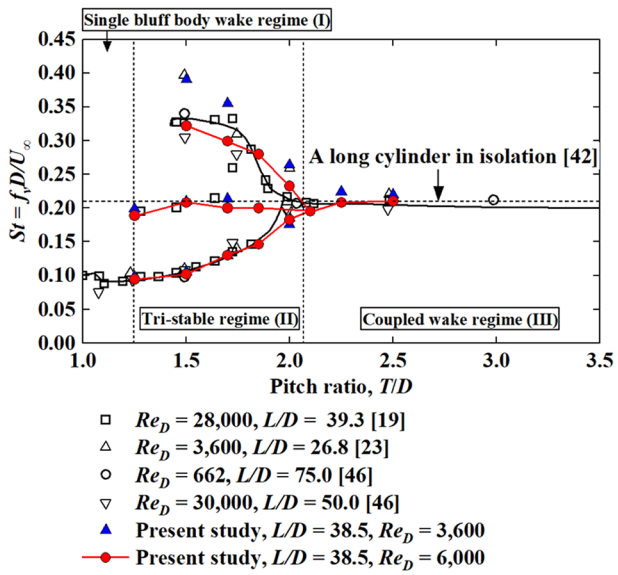


Fig. 7 Wakes shed from two long side-by-side cylinders showing Strouhal number that varies with gap ratio (*T/D*) for selected Reynolds numbers

wakes (i.e., *regime II*) rather than bistable wakes are shed from the two side-by-side cylinders.

3.3 Wake Shedding From Two Short "Stationary" and Flapping Side-by-Side Cylinders. Now, we examine the wake shedding from two short side-by-side cylinders with an aspect ratio of $L/D = 5.0$ whose one end is fixed to the upper wind-tunnel wall. Two configurations to be separately considered include: (a) both short cylinders are stationary thus no vibration (or flapping motion) is generated, and (b) both short cylinders are flappable. By examining the wake shedding frequencies of the two configurations in sequence, we aim to understand how the wake patterns shed from two cylinders with varying gap ratio from $T/D = 1.2$ up to $T/D = 6.0$ are altered by the decreased aspect ratio of $L/D = 5.0$ and the flapping motion at a fixed Reynolds number of $Re_D = 6000$.

3.3.1 Wake Shedding From Two Short Stationary Side-by-Side Cylinders. Results in Fig. 8(*a*) show that the Strouhal number based on the power spectra of two hotwire probe signals measured at positions behind the two stationary cylinders at $T/D = 1.2$, indicated by the inset, exhibits the same peak at $St \sim 0.08$. At a higher gap ratio such as $T/D = 1.4$, two shedding frequencies develop that correspond to the wide (W) and narrow wakes (N), with Strouhal numbers at $St = 0.085$ and 0.3, respectively. Further at $T/D = 1.7$, three dominant peaks of the St co-exist as $St \sim 0.11$ (W), 0.15 (I), and 0.25 (N), respectively, where (I) indicates the intermediate wake structure. At $T/D = 1.9$, three peaks are visible, yet the peak frequency of the narrow wake decreases while that of the wide wake increases. However, the intermediate wake's shedding frequency remains unchanged. At $T/D = 2.2$, two dominant Strouhal numbers peak as $St \sim 0.15$ (I) and 0.21 (N). The peak associated with the wide wake disappears. For $T/D = 2.4$, two dominant Strouhal numbers peak as $St \sim 0.15$ (I) and 0.2 (N). The narrow wake's peak frequency is slightly decreased from that at $T/D = 2.2$. For $T/D = 2.6$, only a single peak appears as $St \sim 0.185$. With the further increased T/D such as $T/D = 4.0$, this single peak's magnitude decreases to $St \sim 0.175$. For $T/D = 6.0$, a single dominant peak of the St exists as $St \sim 0.15$ which corresponds to the intermediate wake's frequency (I).

Based on the data sets presented in Fig. 8(*a*) and more data points at other gap ratios, a new classification of "five" distinct wake shedding patterns is made for short stationary cylinders in a side-by-side arrangement (Fig. 8(*b*)). Description for each regime is detailed as follows.

Regime I corresponds to the single bluff body wake regime, $T/D \le 1.2$, as shown in Figs. 8(*a*) and 8(*b*). The Strouhal number ($St = f_s D/U_\infty \sim 0.08$) is lower than that of two longer cylinders, $St \sim 0.09$ for $L/D = 38.5$ (Fig. 7). This reduction is due to the shortened cylinders generating wakes that are shed at lower rates than the longer cylinders, like the single isolated cylinder discussed in Fig. 6. If the two short cylinders behave like a single bluff body having an equivalent diameter of $D_e = 2D$, the resultant Strouhal number is given as $St = f_s D_e/U_\infty \sim 0.16$ that approximately

Downloaded from http://asmedigitalcollection.asme.org/fluidsengineering/article-pdf/147/5/051301/7413435/fe_147_05_051301.pdf by University of Witwatersrand - Wartewieler Library user on 01 July 2025

correlates to the intermediate Strouhal number of St = 0.15 and the dominant frequency of a single short, isolated cylinder.

Regime II is defined, ranging from $T/D = 1.2$ to $T/D = 1.6$, in which two dominant frequencies are present. Both wide and narrow wakes are shed from the two cylinders and demonstrate their bistability, gap flow switching as indicated by the two dominant frequency components that exist at each side of the cylinders (i.e., solid circle and cross symbols correspond to the upper and lower cylinders, respectively, in Fig. 8(*b*)).

The third regime, regime III, is classified in a gap ratio range of $1.6 \leq T/D < 2.0$. A typical wake shedding behavior in this regime is shown in Figs. 8(*a*) and 8(*b*). Three dominant frequencies co-exist in wakes: higher, intermediate, and lower shedding frequencies. The co-existence of the three dominant frequencies indicates that the wakes are tristable.

Increasing the gap ratio further toward $T/D = 2.0$, the higher and lower Strouhal numbers approach the frequency of the intermediate frequency, $St_{int} \sim 0.15$: the lower St is increased to $St_{int} = 0.15$, while the higher St reduces to 0.2. It should be noted that for the long two-side-by-side arrangement, three dominant Strouhal numbers merged immediately to the intermediate Strouhal number $St_{int} \sim 0.21$ at $T/D \sim 2.2$ (Fig. 7). However, the simultaneous merging of the three distinct wake patterns does not occur for the short cylinders. Rather, the low frequency shed vortices first disappear, leading to *regime IV* where two dominant Strouhal numbers co-exist. Thus, regime IV is defined in the gap ratio range of $2.0 < T/D \leq 2.6$. The lower St corresponds to $St_{int} \sim 0.15$, and this Strouhal number originates from the merged lower St and St_{int} in regime III.

The regime of $T/D > 2.6$ is defined as *regime V*, and St_{int} is suddenly merged into the higher St and thus only the higher St is detected. However, as the gap ratio keeps increasing from which, the higher St gradually decreases to eventually reach St_{int} (Fig. 8(*b*)).

We have established the wake shedding behavior of two side-by-side cylinders based on the Strouhal number variation with gap ratios for the short ($L/D = 5.0$) aspect ratio configuration. Comparing Figs. 7 and 8(*b*), the effect of the reduced aspect ratio is to slightly reduce the wake shedding frequencies, which is consistent

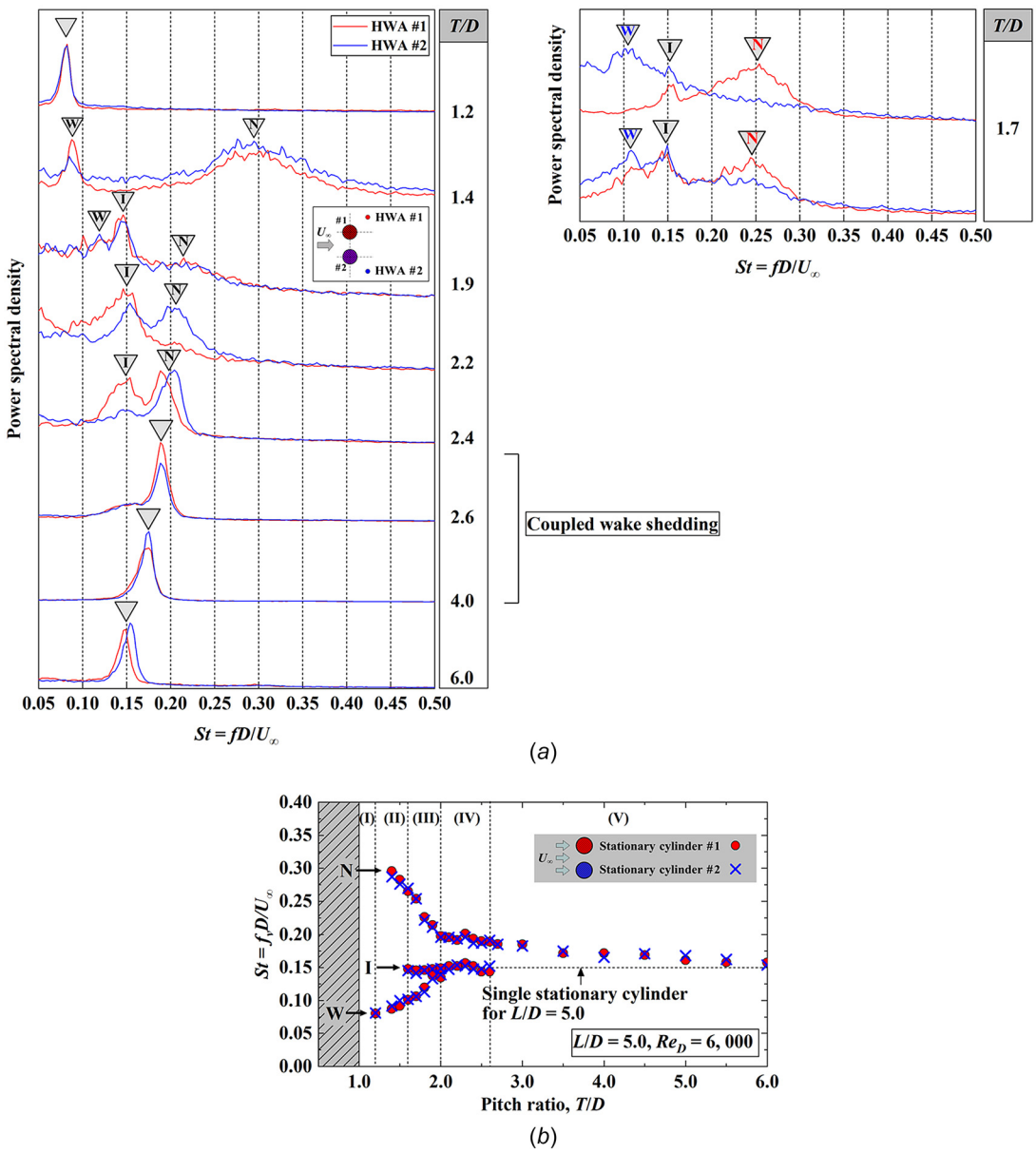


Fig. 8 Wakes shed from two short side-by-side cylinders at $Re_D = 6000$: (*a*) power spectra from both stationary cylinders and (*b*) Strouhal number of both stationary cylinders varying with gap ratio (*T/D*), with a short single stationary cylinder in isolation as reference

Downloaded from http://asmedigitalcollection.asme.org/fluidsengineering/article-pdf/147/5/051301/7413435/fe_147_05_051301.pdf by University of Witwatersrand - Wartewieler Library user on 01 July 2025

with Williamson [45]. However, the short stationary cylinders show the development of another bistability (regime IV) after the tristable regime (see Fig. 8(*b*)), in contrast to the long cylinders where this does not occur (see, Fig. 7).

3.3.2 Wake Shedding From Two Short Flapping Side-by-Side Cylinders. The effects of flapping on the wake patterns shed from two short flappable side-by-side cylinders are examined next, as shown in Fig. 9. The variation of power spectra and corresponding Strouhal numbers with gap ratio is similar to those observed for two short stationary cylinders (see Fig. 8(*b*)), yet with slightly reduced Strouhal numbers for the flapping cantilevers. Figure 10 shows flow visualization of the five wake regimes for two side-by-side short and flapping cylinders. Regime I, ($T/D \leq 1.2$) for a single bluff body regime, is shown in Fig. 10(*a*); regime II, ($1.2 < T/D \leq 1.4$) for the first bistable regime (Fig. 10(*b*)); regime III, ($1.4 < T/D \leq 2.0$) for a tristable regime (Fig. 10(*c*)); regime IV ($2.0 < T/D \leq 2.1$), the second bistable regime (Fig. 10(*d*)); and regime V ($T/D > 2.6$) for a coupled wake regime (Fig. 10(*e*)).

The classification of the wake patterns is similar to the configuration with two short stationary side-by-side cylinders. Yet, subtle differences are made by the flapping motion, where the gap ratio band for the tristable wake regime (i.e., regime III) is broadened.

3.4 Switching Events of Short Flappable Cylinders

3.4.1 Switching Event of Bistable Wakes (Regime II). Further insights into the gap flow switching process for flappable cylinders are obtained from the raw hotwire signal time series shown in Fig. 11. Here, the gap flow is deflected toward cylinder #2, and the narrow wake is formed with the higher St (higher shedding frequency) as visualized by Fig. 10(*b*). On the other hand, a wide wake, "W," is formed behind the other cylinder (cylinder #2) having the lower St. If both wake modes are invariant, it could be regarded as biased wakes. However, the random switching event of these wake modes (N, W) that was observed in Fig. 11 indicates that the wakes are bistable as described by regime II. No other dominant frequency components were detected. In comparison to the case of two stationary side-by-side cylinders, a similar pattern yet with slightly lower shedding frequencies occurs.

3.4.2 Switching Event of Tristable Wakes (Regime III). The co-existence of three dominant wake shedding frequencies in each side of the two side-by-side cylinders in regime III simply means that corresponding three wake patterns of wide, intermediate, and narrow wakes shed from both cylinder's outer cylinder edges as visualized in Fig. 10(*c*).

To examine the correlation of the wakes shed from both cylinders, the sampled hotwire signals at a fixed time window from HWA #1 and #2 are plotted in Fig. 12. By the first hotwire probe (HWA #1) in Fig. 12(*a*), lower frequency signals that correspond to the wide wake (W), St ~ 0.10, were captured, followed by the intermediate

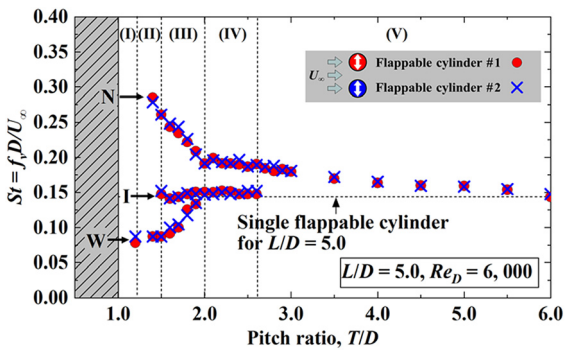


Fig. 9 Strouhal number of both short flapping cylinders varying with gap ratio (*T*/*D*), with a short single flapping cylinder in isolation

frequency signals of intermediate wake (I), St ~ 0.145, and another signal band appears having higher frequencies, corresponding to the narrow wake (N), St ~ 0.24. Simultaneously on the opposite side (HWA #2), higher frequency signals for the narrow wake (N), St ~ 0.24, reciprocal to the wide wake detected by HWA #1 were captured, sequentially followed by intermediate frequency signals, St ~ 0.145, and another signal band appears having lower frequencies, for the wide wake (W), St ~ 0.10. This indicates that the switching process, as W→I→N of cylinder #1's wakes and reciprocal N→I→W of cylinder #2's wakes, occurs. Thus, the wake patterns are tristable, with evidence provided by the flow field visualization shown in Fig. 10(*c*). Further, this switching event takes place from narrow wake to wide wake via intermediate wake or vice versa.

Another switching mode was observed in Fig. 12(*b*). The wide wake (W) is switched to wide wake via intermediate wake (W→I→W) behind cylinder #1 (or HWA #1), while the reciprocal switching process (N→I→N) occurred behind cylinder #2. Only two dominant frequencies exist on each side of the two cylinders that flap in this time window. The switching event shown in Fig. 10(*c*) cannot happen directly between the wide and narrow wake. Rather, the wake switching process occurs via the intermediate wake; thus, direct switching between wide wakes and narrow wakes without involving the intermediate wake was not observed.

3.4.3 Switching Event of Biased Wakes (Regime IV). As the gap ratio is further increased from regime III, another distinct wake shedding pattern features in $2.0 < T/D < 2.6$ as visualized in Fig. 10(*d*). This gap ratio range is termed regime IV. The shed wakes are bistable with the co-existence of two dominant wake shedding frequencies whose sampled hotwire signals from each side of the cylinders are displayed in Fig. 13. The first hotwire probe (HWA #1) captures both intermediate and higher frequency signals that correspond to the intermediate wake (I), St ~ 0.15, and the narrow wake (N), St ~ 0.19, respectively. The second hotwire probe (HWA #2) detects the reciprocal signals, higher frequencies for the narrow wake (N), St ~ 0.19, and intermediate frequencies, St ~ 0.15. However, this bistability involves the switching between the narrow wake and the intermediate wake that has not been observed from the long side-by-side cylinders.

3.4.4 Symmetric Wakes (Regime V). As the gap ratio increases further, i.e., $T/D > 2.6$ (denoted as regime V), a single dominant shedding frequency that used to coincide with the narrow wake in the previous regime (regime IV) only remains. This dominant St value gradually reduces with increasing T/D and eventually approaches the St_{int} as shown in Fig. 9. Now, a question arises as to how these two shedding patterns are coupled despite maintaining the same shedding frequency. It was previously argued [2,24] that either in-phase or antiphase locking still occurs in the symmetric wake regime until a sufficiently large spacing is reached, e.g., $T/D > 4.0$–4.5. The flow images that were visualized in Fig. 10(*e*) confirm the presence of both in-phase or antiphase locking. With $T/D > 4.0$–4.5, the shedding frequencies of the two cylinders are the same but their shedding patterns are completely independent (decoupled).

3.5 Wake Shedding and Flapping of Two Short Side-by-Side Flappable Cylinders. Before proceeding further, we need to understand how the flapping that is induced by the external airstream around each flappable cylinder, in turn, affects the wake patterns as a mutual interaction between the fluid and the structure. To this end, the frequencies measured from periodic wake shedding behind two short flappable cylinders using the hot-wire probes (HWA) and the corresponding flapping frequencies obtained from the piezoelectric plate are plotted in Fig. 14.

The wake shedding frequencies vary linearly with the increasing Reynolds number, within the considered Reynolds number range, indicating a constant Strouhal number for each case. To compare the effect of flapping of two short side-by-side cylinders, reference tests

Downloaded from http://asmedigitalcollection.asme.org/fluidsengineering/article-pdf/147/5/051301/7413435/fe_147_05_051301.pdf by University of Witwatersrand - Wartewieler Library user on 01 July 2025

were also performed using single short cylinders in *isolation*, i.e., one stationary (nonflapping) cylinder and individual flappable cylinders #1 (Fig. 14(*a*)) and #2 (Fig. 14(*b*)). It is apparent that the flapping slightly reduces wake shedding frequencies (f_s).

With two flappable cylinders positioned in the side-by-side arrangement, three frequency branches are measured behind each cylinder, as shown by the three circular dots in Figs. 14(*a*) and 14(*b*), indicating the tristability of the wakes as previously discussed in Fig. 12 for regime III at $T/D = 1.7$. The intermediate wakes are shed at the same frequencies as those behind the isolated flapping cylinder. At the same time, wakes are shed at higher and lower frequencies, respectively, representing narrow and wide wakes.

These wakes are shed at different frequencies and simultaneously induce the flapping of both cylinders. The flapping signals shown in Fig. 14 acquired from the piezo-sensors attached to each of the cylinder's mounting base depict clearly that the flapping (f_f) occurs at their natural frequencies (31 Hz for flappable cylinder #1 and 30 Hz for flappable cylinder #2). It is important to note that natural frequency (f_n) invariance is evident, regardless of fluidic configurations such as in isolation, or in the side-by-side arrangement, and Reynolds numbers. In particular, the Reynolds number independent flapping of both cylinders has a negligible impact on the wake shedding frequencies due to a large contrast in the flappable cylinder-to-fluid mass ratio.

Figure 14(*c*) shows the RMS signals from the piezo-sensors attached to the mounting base of flappable cylinder #1. While the flapping frequencies are constant regardless of the Reynolds numbers (Fig. 14(*a*)), the flapping displacement (that is linearly related to the PZT plate output voltage) increases with Reynolds number (Fig. 14(*c*)). The increased Reynolds number means faster wake (vortex) shedding. Thus, the vortex shedding frequency approaches the natural frequency of flappable cylinder #1 as the

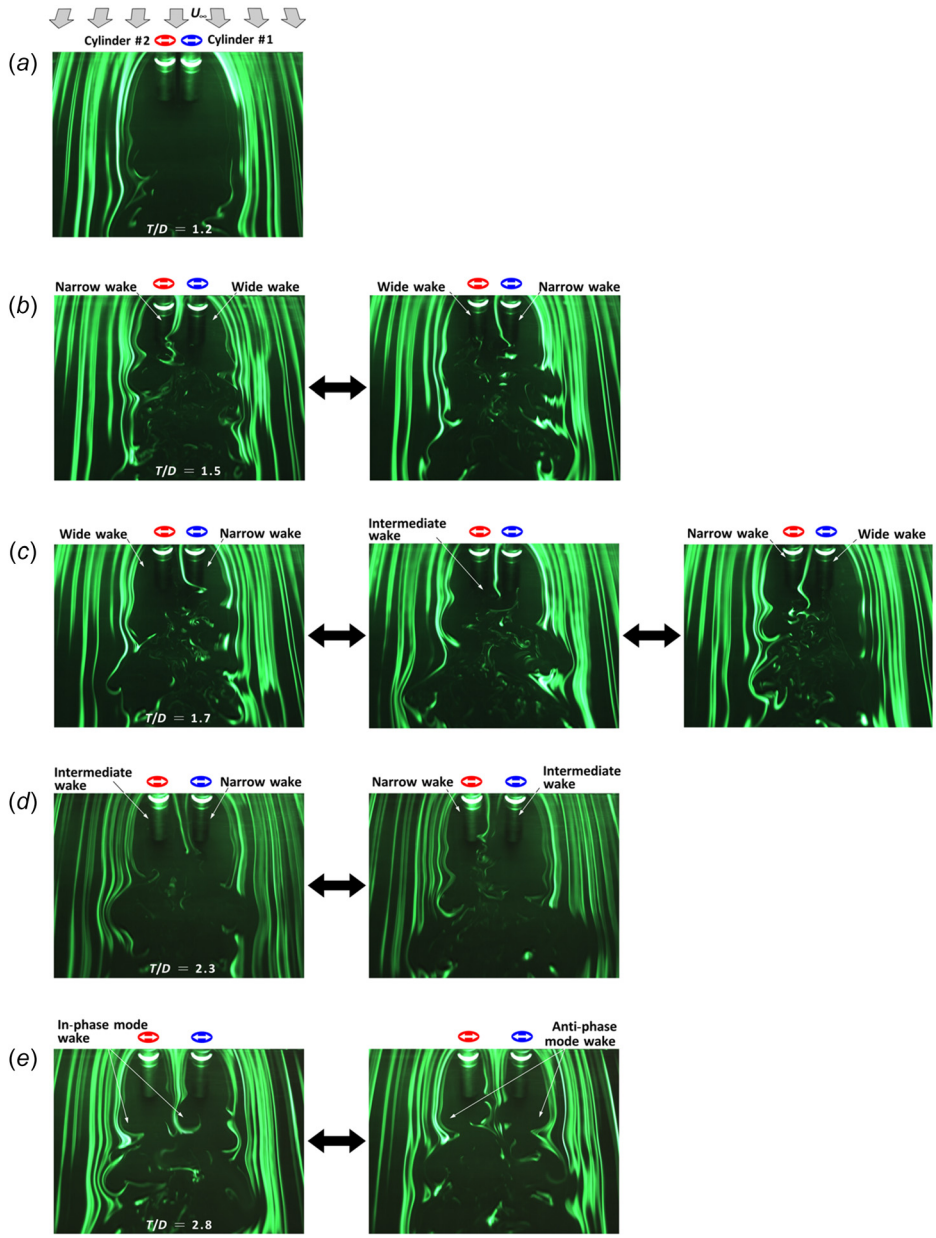


Fig. 10 Visualized wake patterns behind both flapping cylinders, distinctively varying with gap ratio (T/D) all at $Re_D = 1800$ where the flow direction is from top to bottom: (*a*) single bluff body wake regime (regime I, $T/D = 1.2$), (*b*) first bistable wake regime (regime II, $T/D = 1.4$), (*c*) tristable wake regime (regime III, $T/D = 1.7$), (*d*) second bistable wake regime (regime IV, $T/D = 2.3$), and (*e*) coupled (in-phase mode wake and antiphase wake) regime (regime V, $T/D = 2.8$)

Downloaded from http://asmedigitalcollection.asme.org/fluidsengineering/article-pdf/147/5/051301/7413435/fe_147_05_051301.pdf by University of Witwatersrand - Wartewieler Library user on 01 July 2025

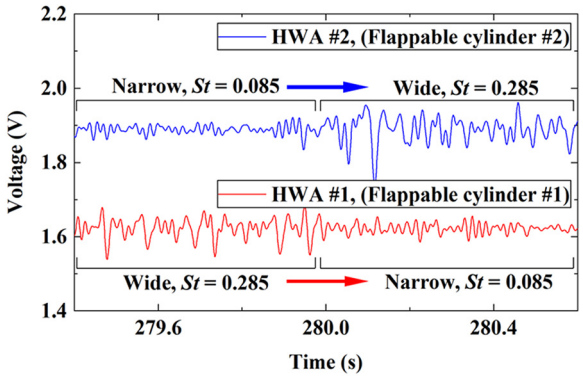


Fig. 11 Bistable wakes that switch at $T/D = 1.4$ and $Re_D = 6000$ by sampled raw voltage signals from HWA#1 showing the switching from wide (W) wakes to narrow (N) wakes, i.e., W→N, and from HWA#2 showing the reciprocal switching from narrow (N) wakes to wide (W) wakes N→W

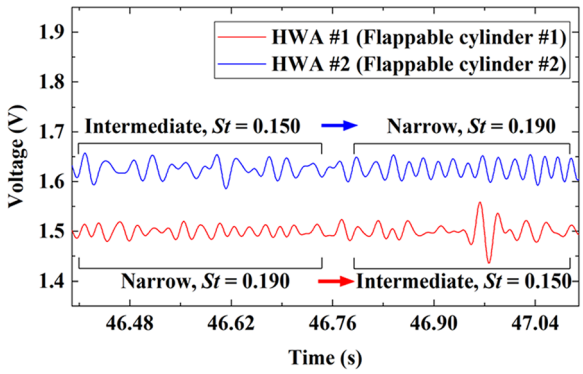


Fig. 13 Biased wakes shed at $T/D = 2.3$ and $Re_D = 6000$ by sampled raw voltage signals from HWA #1 and HWA #2, showing the biased switching mode, i.e., N→I for flappable cylinder #1 and I→N for flappable cylinder #2

Reynolds number is increased from 3200. With resonance at the natural frequency, the power output from the piezo-sensor locally peaks at $Re_D = 6000$ (i.e., $U_r = 5.9$), followed by a drop and then a monotonic increase as the Reynolds number is increased further due to galloping similarly observed by Sun et al. [47] and Gao and Wan [48]. In comparison to the flappable cylinder in isolation, the magnitude of the local peak power output due to resonance is reduced when the flappable cylinders are arranged in a side-by-side configuration. Further, the resonance occurs only at the intermediate shedding frequency for $Re_D = 6350$ (i.e., $U_r = 6.4$), for example, as shown in Fig. 14(*a*), whereby the intermediate frequency "circular dot" overlays the flapping and natural frequency line. Thus, there is no sign of resonance caused by the flapping frequency of cylinders matching the shedding frequency of the narrow and wide wakes.

3.6 Synchronization Between Flapping Cylinders and the Wake Shedding. Thus far, we have examined how the flapping and vortex shedding are interactively connected. Now, we consider in greater detail how the flapping of the two cylinders in a side-by-side arrangement is coupled, where a piezo output signal is linearly related to the displacement of a cylinder. Here, we analyzed the mode shapes (i.e., in-phase or antiphase) of flapping cylinders by processing the piezo-signals using a quantitative parameter, i.e., the correlation coefficient. The correlation coefficient is a numerical measure of the strength of two variables, which quantifies the degree of linear association between the ranks of two signal data sets. It ranges from −1 to +1 where values closer to −1 (antiphase mode) or +1 (in-phase mode) represent a stronger degree of linear dependence than those closer to 0.

One of the useful definitions for the correlation coefficient is Spearman's correlation coefficient r_s [49]. Let $u_1, u_2, u_3, \ldots, u_n$ denote the ranks of "n" observed values of signal X, and let $v_1, v_2, v_3, \ldots, v_n$ denote the ranks of n observed values of signal Y. The Spearman coefficient r_s can be defined by

$$r_s = \frac{S_{uv}}{\sqrt{S_u^2 S_v^2}} \tag{7}$$

where S_{uv} is the sample covariance between the u and v, S_u^2 is the sample variance of the u, and S_u^2 is the sample variance of the v.

As summarized in Table 1, the correlation coefficient between the two flapping cylinders, i.e., $r_{s\,\mathrm{F\text{–}F}}$, calculated by Eq. (7), based on the piezo-signals (Fig. 15) acquired for any given 1.5 s exhibits an absolute value close to 0. Thus, indicating that the two flapping cylinders are neither in-phase nor antiphase, regardless of the gap ratios, $T/D = 1.2, 1.7, 2.3, 2.8$, and 6.0. Since the flapping for the two side-by-side cylinders is confirmed not to be obviously coupled, a question arises as to whether the flapping is correlated with the wake shedding. The synchronization between the flapping and the wake shedding are further examined by the Spearman correlation coefficient $r_{s\,\mathrm{F\text{–}S}}$ calculated from the piezo-signal of flapping cylinder #2 in the side-by-side arrangement and the HWA signal simultaneously recorded behind it, respectively. Here, the synchronization between hot-wire signals and PZT signals was carried out

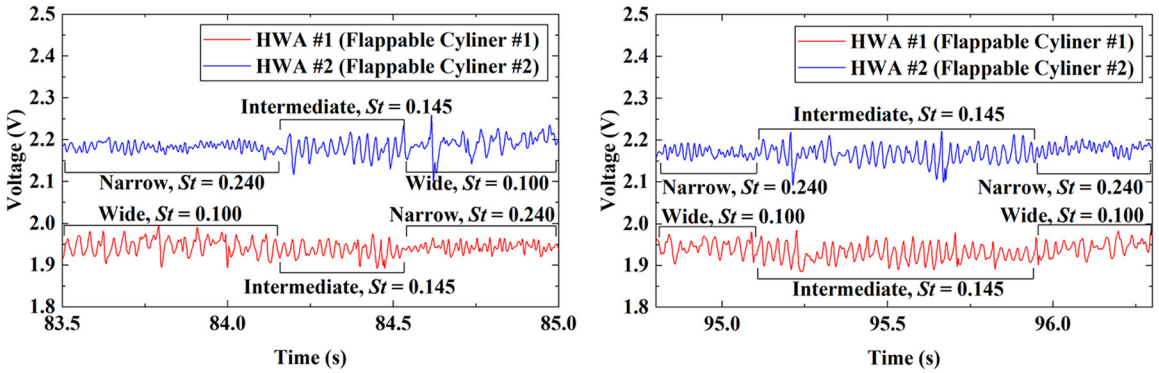


Fig. 12 Tristable wakes shed at $T/D = 1.7$ and $Re_D = 6000$ (i.e., regime III): (*a*) sampled raw voltage signals from HWA #1 and HWA #2, showing the full switching mode, i.e., W→I→N for flappable cylinder #1 and N→I→W for flappable cylinder #2 and (*b*) sampled raw voltage signals from HWA #1 and HWA #2, showing the biased switching mode, i.e., W→I→W for flappable cylinder #1 and N→I→N for flappable cylinder #2

Downloaded from http://asmedigitalcollection.asme.org/fluidsengineering/article-pdf/147/5/051301/7413435/fe_147_05_051301.pdf by University of Witwatersrand - Wartewelier Library user on 01 July 2025

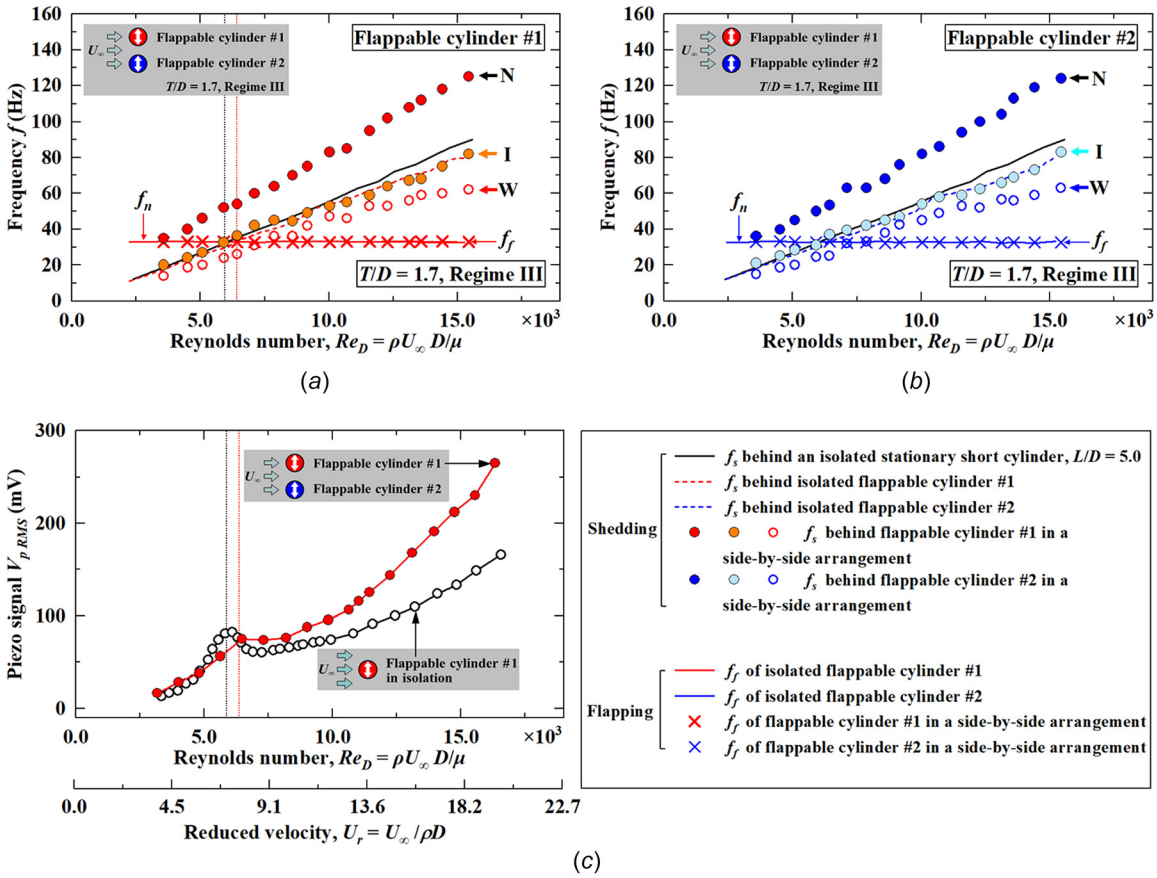


Fig. 14 Wake shedding frequency (f_s) and flapping frequency (f_f) at $T/D = 1.7$, as a function of Reynolds number: (*a*) for flappable cylinder #1, (*b*) for flappable cylinder #2, and (*c*) piezo-signals showing amplification due to resonance

by the data acquisition system (CTA-Streamware Pro MultiCal) in 60 s at the sampling rate of 10 kHz. Based on the synchronized signals from the hot-wire anemometers and PZT sensors, the calculated $r_{s\,\mathrm{F–S}}$ at differing gap ratio and Reynolds number is shown to be close to 0 (Table 2), indicating a negligible synchronization between the flapping and the wake shedding.

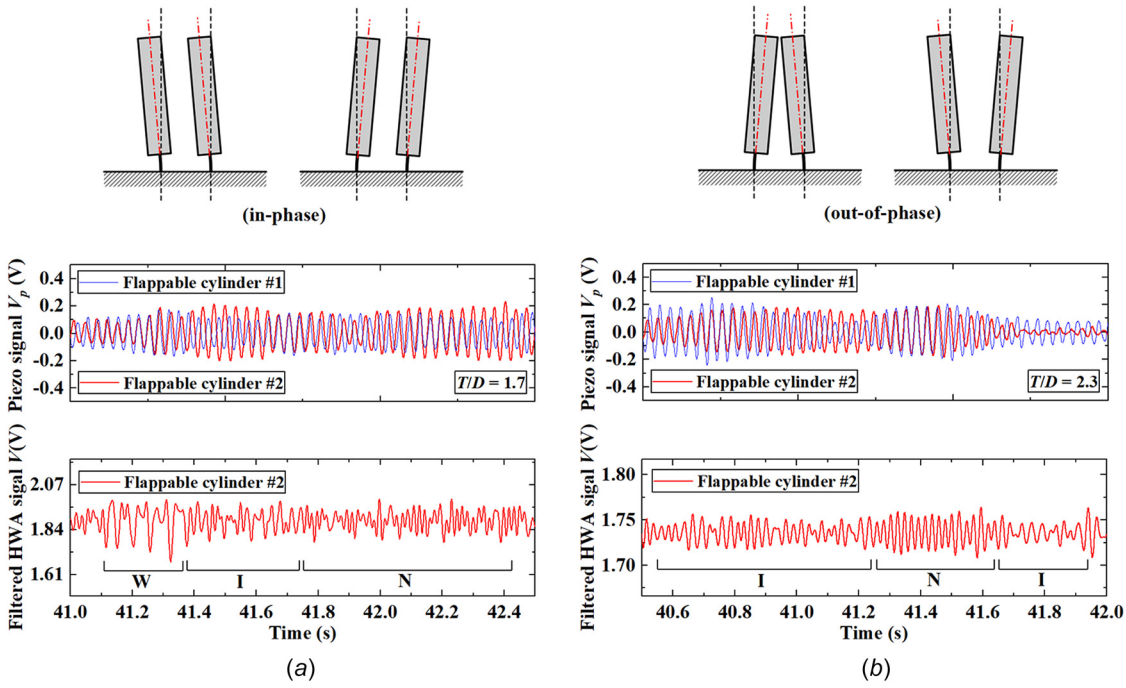


Fig. 15 Time-resolved signals from both PZT mounts attached to the base of each flappable cylinder and the corresponding switching events of wakes shed at $Re_D = 6000$: (*a*) at $T/D = 1.7$ and (*b*) at $T/D = 2.3$

Downloaded from http://asmedigitalcollection.asme.org/fluidsengineering/article-pdf/147/5/051301/7413435/fe_147_05_051301.pdf by University of Witwatersrand - Wartewieler Library user on 01 July 2025

Table 1 Flapping–flapping correlation coefficient of the piezo-signals from both flappable cylinder #1 and flappable cylinder #2 in a side-by-side arrangement, $r_{s\ \mathrm{F–F}}$

Re_D	$T/D = 1.2$	1.7	2.3	2.8	6.0
3600	0.03854	−0.03902	−0.03802	0.01797	0.03056
6000	0.03685	−0.013118	−0.01249	0.0215	0.0714
8100	−0.01312	0.01007	−0.00238	0.03364	−0.02239
10,500	0.03389	−0.01837	0.02671	0.00329	−0.00988

Table 2 Flapping–shedding correlation coefficient of the piezo-signal from flappable cylinder #2 and the hot-wire signals from HWA#2 in a side-by-side arrangement, $r_{s\ \mathrm{F–S}}$

Re_D	$T/D = 1.2$	1.7	2.3	2.8	6.0
3600	−0.03931	−0.04412	0.07718	−0.02116	−0.04944
6000	−0.03491	−0.00306	0.07085	0.02172	0.03029
8100	0.03361	0.06619	0.04212	0.05283	−0.00017
10,500	0.02942	0.0721	0.03472	−0.00878	0.004007

Thus, we may conclude that there is no apparent coupling between (i) two flapping cylinders and (ii) a flapping cylinder and the shed wakes in our setup. However, strong coupling was reported by previous studies when resonance occurred for longer two side-by-side cylinders: in-phase vibration within the single bluff body regime [10,14] and both antiphase and in-phase vibration in the bistable wake flow regime [10,37]. We believe that the strong coupling observed in these studies was attributed to a small cylinder-to-fluid mass ratio. In contrast, the setup in this study is characterized by a large cylinder-to-fluid mass ratio (e.g., $m^* = 1240$ and 1330), which keep the cylinder vibration frequencies invariant (i.e., $f_f \approx f_n$) as the Reynolds numbers increase (see Figs. 14(*a*) and 14(*b*)). In addition, the lock-in phenomenon occurred only within a narrow frequency range near the natural frequency of each flappable cylinder. Thus, the present cylinders with the large m^* have a negligible correlation to the wake shedding, unlike the strong correlation observed with the low m^* values, e.g., $m^* \leq 565$ [10,14].

4 Conclusions

We experimentally characterized wake shedding and switching events of two short flapping cylinders in a side-by-side arrangement. The new findings are summarized as follows: (1) The shortness of stationary or flappable cylinders (i.e., length-to-diameter ratio) reduces the magnitude of wake shedding frequencies. A further reduction occurs when both short cylinders flap. (2) On the basis of wake shedding frequencies, distinct wake regimes are classified by the gap ratio, sequentially transitioning from a single bluff body, bistable wakes, tristable wakes, another bistable wakes, coupled wakes and eventually to uncoupled wakes. This classification is commonly made for stationary and flappable two short side-by-side cylinders. (3) The dominant frequency of vortices shed in wide wakes for the tristable wake regime first merges with that of intermediate wakes, which corresponds to both short stationary and flappable cylinders in isolation. With a further increased T/D, the two dominant vortex shedding frequencies in intermediate and narrow wakes co-exist until the narrow wakes eventually merge into the intermediate wakes. (4) Multiple wake shedding patterns co-exist with the switching. Unlike the direct switching between two wake patterns of the bistable wakes regimes, the switching events of shed wakes in the tristable regime take place from narrow wakes to wide wakes via intermediate wakes or vice versa. The direct switching between wide wakes and narrow wakes without involving the intermediate wake was not observed. (5) Within the Reynolds number range considered, the cylinders always flap at their natural frequency regardless of their fluidic configurations; in isolation and in a side-by-side arrangement, and Reynolds numbers. The flapping negligibly influences the wake shedding characteristics such as shedding frequencies and switching events, due to the large contrast of flappable cylinder-to-fluid mass ratio (i.e., negligible synchronization).

Funding Data

- National Natural Science Foundation of China (NSFC) (Nos. 11972185 and 12032010; Funder ID: 10.13039/501100001809).

Data Availability Statement

The datasets generated and supporting the findings of this article are obtainable from the corresponding author upon reasonable request.

Nomenclature

a = distance between the cylinder bluff body to the base, m
A = dimensionless coefficient of King's law
B = dimensionless coefficient of King's law
D = cylinder diameter, m
D_e = equivalent cylinder diameter, m
E = voltage signal of hot-wire probe, mV
f_f = flapping frequency of the flapping cylinder, Hz
f_n = natural frequency of the flapping cylinder, Hz
f_s = wake shedding frequency, Hz
h = test section height, m
L = cylinder length, m
m = mass of the flapping cylinder, kg
m^* = cylinder-to-fluid mass ratio
r_s = Spearman's correlation coefficient
$r_{s\ \mathrm{F–F}}$ = Spearman's correlation coefficient between the flapping of two flapping cylinders
$r_{s\ \mathrm{F–S}}$ = Spearman's correlation coefficient between the flapping and wake shedding of a flapping cylinder
Re_D = Reynolds number
S_i = standard deviation of the signal component X_i
S_{ij} = sample covariance between the signal component X_i and X_j
St = Strouhal number
$\mathrm{St}_{\mathrm{int}}$ = Strouhal number of intermediate wakes
t = time, s
T = center to center distance of cylinders, m
T_i = turbulence intensity
$\overline{U}$ = time-averaged velocity, m s^{-1}
U_C = mean mainstream velocity in the middle of test section, m s^{-1}
U_r = reduced velocity
U_{RMS} = root-mean-square of mainstream velocity, m s^{-1}
U_∞ = mean mainstream velocity, m s^{-1}
V_p = voltage signal of piezoelectric sensor, V
$V_{p,\mathrm{RMS}}$ = root-mean-square piezo-signal, V
w = test section width, m
ε = cylinder flapping angle, deg
$\varepsilon_{\mathrm{RMS}}$ = RMS value of the cylinder flapping angle, deg
ξ = damping of the flapping cylinder
ρ = density of cylinder, kg/m^3

References

[1] Zdravkovich, M. M., 1977, "Review of Flow Interference Between Two Circular Cylinders in Various Arrangement," ASME J. Fluids Eng., **99**(4), pp. 618–633.
[2] Sumner, D., Wong, S. S. T., Price, S. J., and Paidoussis, M. P., 1999, "Fluid Behavior of Side-by-Side Circular Cylinders in Steady Cross-Flow," J. Fluids Struct., **13**(3), pp. 309–338.
[3] Wang, J., Fan, D., and Lin, K., 2020, "A Review on Flow-Induced Vibration of Offshore Circular Cylinder," J. Hydrodyn., **32**(3), pp. 415–440.
[4] Lee, Y. J., Qi, Y., Zhou, G., and Lua, B. K., 2019, "Vortex-Induced Vibration Wind Energy Harvesting by Piezoelectric MEMS Device in Formation," Sci. Rep., **9**, p. 20404.

Downloaded from http://asmedigitalcollection.asme.org/fluidsengineering/article-pdf/147/5/051301/7413435/fe_147_05_051301.pdf by University of Witwatersrand - Wartewelier Library user on 01 July 2025

[5] Brun, C., Tenchine, D., and Hopfinger, E. J., 2004, "Role of the Shear Layer Instability in the Near Wake Behavior of Two Side-by-Side Circular Cylinders," Exp. Fluids, **36**(2), pp. 334–343.
[6] Atkins, M. D., Dala, L., and Kim, T., 2016, "Time-Averaged Behavior of Gap Flow Between Two Side-by-Side Circular Cylinders," AIAA J., **54**(9), pp. 2742–2754.
[7] Graham, J. M. R., 1969, "The Effect of End-Plates on the Two-Dimensionality of a Vortex Wake," Aeronaut. Q., **20**(3), pp. 237–247.
[8] Okamoto, T., and Yagita, M., 1973, "The Experimental Investigation on the Flow Past a Circular Cylinder of Finite Length Placed Normal to the Plane Surface in a Uniform Stream," Bull. JSME, **16**(95), pp. 805–814.
[9] Chakroun, W. M., Abdel Rahman, A. A., and Quadri, M. M. A., 1997, "The Effect of Surface Roughness on Flow Around a Circular Cylinder," Wind Eng., **21**(1), pp. 1–12.
[10] Kim, S., and Alam, M. M., 2015, "Characteristics and Suppression of Flow-Induced Vibrations of Two Side-by-Side Circular Cylinders," J. Fluids Struct., **54**, pp. 629–642.
[11] Wang, X. Q., So, R. M. C., Xie, W.-C., and Zhu, J., 2008, "Free-Stream Turbulence Effects on Vortex-Induced Vibration of Two Side-by-Side Elastic Cylinders," J. Fluids Struct., **24**(5), pp. 664–679.
[12] Xu, S. J., Zhou, Y., and So, R. M. C., 2003, "Reynolds Number Effects on the Flow Structure Behind Two Side-by-Side Cylinders," Phys. Fluids, **15**(5), pp. 1214–1219.
[13] Bearman, P. W., and Wadcock, A. J., 1973, "The Interaction Between a Pair of Circular Cylinders Normal to a Stream," J. Fluid Mech., **61**(3), pp. 499–511.
[14] Zdravkovich, M. M., 1985, "Flow Induced Oscillations of Two Interfering Circular Cylinders," J. Sound Vib., **101**(4), pp. 511–521.
[15] Wang, Z. J., and Zhou, Y., 2005, "Vortex Interaction in a Two Side-by-Side Cylinder Near-Wake," Int. J. Heat Fluid Flow, **26**(3), pp. 362–377.
[16] Alam, M. M., and Zhou, Y., 2007, "Flow Around Two Side-by-Side Closely Spaced Circular Cylinders," J. Fluids Struct., **23**(5), pp. 799–805.
[17] Sumner, D., 2010, "Two Circular Cylinders in Cross-Flow: A Review," J. Fluids Struct., **26**(6), pp. 849–899.
[18] Chen, W., Ji, C., Alam, M. M., and Yan, Y., 2022, "Three-Dimensional Flow Past Two Stationary Side-by-Side Circular Cylinders," Ocean Eng., **244**(15), p. 110379.
[19] Alam, M. M., Moriya, M., and Sakamoto, H., 2003, "Aerodynamic Characteristics of Two Side-by-Side Circular Cylinders and Application of Wavelet Analysis on the Switching Phenomenon," J. Fluids Struct., **18**(3–4), pp. 325–346.
[20] Spivack, H. M., 1946, "Vortex Frequency and Flow Pattern in the Wake of Two Parallel Cylinders at Varied Spacing Normal to an Air Stream," J. Aeronaut. Sci., **13**(6), pp. 289–301.
[21] Afgan, I., Kahil, Y., Benhamadouche, S., and Sagaut, P., 2011, "Large Eddy Simulation of the Flow Around Single and Two Side-by-Side Cylinders at Subcritical Reynolds Numbers," Phys. Fluids, **23**(7), p. 075101.
[22] Zhou, Y., Zhang, H. J., and Yiu, M. W., 2002, "The Turbulent Wake of Two Side-by-Side Circular Cylinders," J. Fluid Mech., **458**, pp. 303–332.
[23] Kim, H. J., and Durbin, P. A., 1988, "Investigation of the Flow Between a Pair of Circular Cylinders in the Flopping Regime," J. Fluid Mech., **196**, pp. 431–448.
[24] Williamson, C. H. K., 1985, "Evolution of a Single Wake Behind a Pair of Bluff Bodies," J. Fluid Mech., **159**, pp. 1–18.
[25] Rooney, D. M., Rodichok, J., and Dolan, K., 1995, "Finite Aspect Ratio Effects on Vortex Shedding Behind Two Cylinders at Angles of Incidence," ASME J. Fluids Eng., **117**(2), pp. 219–226.
[26] Sarpkaya, T., 1979, "Vortex-Induced Oscillations: A Selective Review," ASME J. Appl. Mech., **46**(2), pp. 241–258.
[27] Irawan, Y. H., Raza, S. A., and Chern, M., 2022, "Numerical Predictions of Vibration Responses and Flow Energy Conversion Efficiency of Side-by-Side Cylinders at Moderate Reynolds Number," Appl. Ocean Res., **129**, p. 103392.
[28] Dahl, J. M., Hover, F. S., Triantafyllou, M. S., Dong, S., and Karniadakis, G. E., 2007, "Resonant Vibrations of Bluff Bodies Cause Multivortex Shedding and High Frequency Forces," Phys. Rev. Lett., **99**(14), p. 144503.
[29] Bearman, P. W., 2011, "Circular Cylinder Wakes and Vortex-Induced Vibrations," J. Fluids Struct., **27**(5–6), pp. 648–658.
[30] Sarpkaya, T., 2004, "A Critical Review of the Intrinsic Nature of Vortex-Induced Vibrations," J. Fluids Struct., **19**(4), pp. 389–447.
[31] Williamson, C. H. K., and Govardhan, R., 2008, "A Brief Review of Recent Results in Vortex-Induced Vibrations," J. Wind Eng. Ind. Aerodyn., **96**(6–7), pp. 713–735.
[32] Dyrbye, C., and Hansen, S. O., 1997, *Wind Loads on Structures*, Wiley, Hoboken, NJ.
[33] Feng, C. C., 1968, "The Measurement of Vortex Effects in Flow Past Stationary and Oscillating Circular and D-Section Cylinders," M.A.Sc. thesis, University of British Columbia, Vancouver, BC, Canada.
[34] Bearman, P. W., 1984, "Vortex Shedding From Oscillating Bluff Bodies," Annu. Rev. Fluid Mech., **16**(1), pp. 195–222.
[35] Williamson, C. H. K., and Govardhan, R., 2004, "Vortex Induced Vibrations," Annu. Rev. Fluid Mech., **36**(1), pp. 413–455.
[36] Parkinson, G. V., 1974, "Mathematical Models of Flow-Induced Vibrations of Bluff Bodies," *Flow Induced Structural Vibrations*, E. Naudascher, ed., Springer, Berlin, Germany.
[37] Quadflieg, H., 1977, "Vortex-Induced Forces on a Pair of Circular Cylinders in Incompressible High Reynolds Number Flow," Forsch. Ingenieurwes., **43**, pp. 9–18.
[38] Zhou, Y., Wang, Z. J., So, R. M. C., Xu, S. J., and Jin, W., 2001, "Free Vibrations of Two Side-by-Side Cylinders in a Cross-Flow," J. Fluid Mech., **443**, pp. 197–229.
[39] King, L. V., 1914, "On the Convection of Heat From Small Cylinders in a Stream of Fluid: Determination of the Convective Constants of Small Platinum Wires With Applications to Hot Wire Anemometry," Proc. R. Soc. London A, **90**(622), pp. 563–570.
[40] Collis, D. C., and Williams, M. J., 1959, "Two-Dimensional Convection From Heated Wires at Low Reynolds Numbers," J. Fluid Mech., **6**(3), pp. 357–384.
[41] Coleman, H. W., and Steele, W. G., 2018, *Experimentation, Validation, and Uncertainty Analysis for Engineers*, **3**rd ed., Wiley, Hoboken, NJ.
[42] Roshko, A., 1953, "On the Development of Turbulent Wakes From Vortex Streets," National Advisory Committee for Aeronautics, Washington, DC, Report No. NACA-TN-2913.
[43] Farivar, D., 1981, "Turbulent Uniform Flow Around Cylinders of Finite Length," AIAA J., **19**(3), pp. 275–281.
[44] Sakamoto, H., and Arie, M., 1983, "Vortex Shedding From a Rectangular Prism and a Circular Cylinder Placed Vertically in a Turbulent Boundary Layer," J. Fluid Mech., **126**, pp. 147–165.
[45] Williamson, C. H. K., 1989, "Oblique and Parallel Modes of Vortex Shedding in the Wake of a Circular Cylinder at Low Reynolds Numbers," J. Fluid Mech., **206**, pp. 579–627.
[46] Kamemoto, K., 1976, "Formation and Interaction of Two Parallel Vortex Streets," Bull. JSME, **19**(129), pp. 283–290.
[47] Sun, H., Kim, E. S., Nowakowski, G., Mauer, E., and Bernitsas, M. M., 2016, "Effect of Mass-Ratio, Damping, and Stiffness on Optimal Hydrokinetic Energy Conversion of a Single, Rough Cylinder in Flow Induced Motions," Renewable Energy, **99**, pp. 936–959.
[48] Gao, X., Shih, W.-H., and Shih, W. Y., 2013, "Flow Energy Harvesting Using Piezoelectric Cantilevers With Cylindrical Extension," IEEE Trans. Ind. Electron., **60**(3), pp. 1116–1118.
[49] Looney, S. W., and Hagan, J. L., 2011, "Statistical Methods for Assessing Biomarkers and Analyzing Biomarker Data," Handb. Stat., **27**, pp. 27–65.

Downloaded from http://asmedigitalcollection.asme.org/fluidsengineering/article-pdf/147/5/051301/7413435/fe_147_05_051301.pdf by University of Witwatersrand - Wartewieler Library user on 01 July 2025